ISSN 1674-1056
http://cpb.iphy.ac.cn
http://iopscience.iop.org/cpb
中国物理 B
Chinese Physics
中国物理 Chinese Physics B

Experimental determination of distributions of soot particle diameter and number density by emission and scattering techniques

Huawei Liu(柳华蔚), Shu Zheng(郑树)

Citation: Chin. Phys. B . 2019, 28(1): 014206. **doi:** 10.1088/1674-1056/28/1/014206
Journal homepage: http://cpb.iphy.ac.cn; http://iopscience.iop.org/cpb

What follows is a list of articles you may be interested in

Geometrical condition for observing Talbot effect in plasmonics infinite metallic groove arrays

Afshari-Bavil Mehdi, Xiao-Ping Lou(娄小平), Ming-Li Dong(董明利), Chuan-Bo Li(李传波), Shuai Feng(冯帅), Parsa Saviz, Lian-Qing Zhu(祝连庆)

Chin. Phys. B . 2018, 27(12): 124204. **doi:** 10.1088/1674-1056/27/12/124204

Super-resolution imaging via sparsity constraint and sparse speckle illumination

Pengwei Wang(王鹏威), Wei Li(李伟), Chenglong Wang(王成龙), Zunwang Bo(薄遵望), Wenlin Gong(龚文林)

Chin. Phys. B . 2018, 27(7): 074202. **doi:** 10.1088/1674-1056/27/7/074202

Passive ranging and a three-dimensional imaging system through wavefront coding

Xing-Xu Zhang(张星煦), Lei Qiao(乔磊), Ting-Yu Zhao(赵廷玉), Rong-Sheng Qiu(仇荣生)

Chin. Phys. B . 2018, 27(5): 054205. **doi:** 10.1088/1674-1056/27/5/054205

Optical encryption of multiple three-dimensional objects based on multiple interferences and single-pixel digital holography

Ying Wang(王莹), Qi Liu(刘琦), Jun Wang(王君), Qiong-Hua Wang(王琼华)

Chin. Phys. B . 2018, 27(3): 034202. **doi:** 10.1088/1674-1056/27/3/034202

Reflective ghost imaging free from vibrating detectors

Heng-xing Li(李恒星), Yan-feng Bai(白艳锋), Xiao-hui Shi(施晓辉), Su-qin Nan(南苏琴), Li-jie Qu(屈利杰), Qian Shen(沈倩), Xi-quan Fu(傅喜泉)

Chin. Phys. B . 2017, 26(10): 104204. **doi:** 10.1088/1674-1056/26/10/104204

Experimental determination of distributions of soot particle diameter and number density by emission and scattering techniques*

Huawei Liu(柳华蔚)† and Shu Zheng(郑树)

Key Laboratory of Condition Monitoring and Control for Power Equipment (Ministry of Education), School of Energy, Power and Mechanical Engineering, North China Electric Power University, Beijing 102206, *China*

(Received 25 July 2018; revised manuscript received 24 August 2018; published online 12 December 2018)

A diagnostics method was presented that uses emission and scattering techniques to simultaneously determine the distributions of soot particle diameter and number density in hydrocarbon flames. Two manta G-504C cameras were utilized for the scattering measurement, with consideration of the attenuation effect in the flames according to corresponding absorption coefficients. Distributions of soot particle diameter and number density were simultaneously determined using the measured scattering coefficients and absorption coefficients under multiple wavelengths already measured with a SOC701V hyper-spectral imaging device, according to the Mie scattering theory. A flame was produced using an axisymmetric laminar diffusion flame burner with 194 mL/min ethylene and 284 L/min air, and distributions of particle diameter and number density for the flame were presented. Consequently, the distributions of soot volume fraction were calculated using these two parameters as well, which were in good agreement with the results calculated according to the Rayleigh approximation, demonstrating that the proposed diagnostic method is capable of simultaneous determination of the distributions of soot particle diameter and number density.

Keywords: soot particle diameter, soot particle number density, soot volume fraction, scattering measurement

PACS: 42.30.–d, 42.68.Ay **DOI:** 10.1088/1674-1056/28/1/014206

1. Introduction

Soot particles are prevalent in the combustion process of hydrocarbon fuel. The study of soot particles in combustion flames benefits the promotion of combustion efficiency and the development of combustion theory and technology. Many properties of particles depend on the particle sizes. Therefore, measurement of particle size in combustion flames is of great research value and significance.

Available measurement techniques of particle size include the optical[1–10] and the non-optical measurement techniques.[5,11–14] Due to the non-intrusion characteristic, real-time capability, and convenience of simultaneous multi-dimension measurement, optical methods have been used by numerous researchers for the measurement of particle parameters. Laser-induced incandescence (LII) is one of the most popular optical techniques, in which soot volume fraction can be determined by the LII signal intensity.[1–6,8,10,15] What is more, primary-particle sizes can also be determined based on the particle-cooling rate after laser heating with pulsed LII, using the time-resolved LII technique (TiRe-LII).[6,8] The determination of particle sizes involves many models accounting for the particle heating by absorption and cooling by conduction, sublimation, radiation, and other effects, different choices of which will lead to large variability of measurement results.[6,8] Nevertheless, determination of particle sizes and gas temperatures simultaneously is still a difficult problem.[2,10] Rayleigh-scattering and Laser-induced incandescence in combination with the detection of the extinction using one single laser pulse (RAYLIX) is another optical technique to measure particle sizes.[1,3] In this technique, combination of scattering, extinction, and LII techniques is used to determine particle sizes, which are essentially calculated using coefficients of absorption and scattering. Emission based techniques are common methods to measure distributions of temperature and absorption coefficient,[16–26] which can help to determine particle sizes in the replacement of the extinction and LII techniques in the RAYLIX with much simpler experimental system and lower cost. Yan *et al.* presented the two-dimensional (2-D) distributions of temperature and soot volume fraction using charge-coupled device (CCD) cameras, with consideration of the broad response spectrum,[20] or using a double-bandpass filter.[24] Ni *et al.*[22] captured the multispectral flame images using CCD cameras with liquid crystal tunable filters, and retrieved the temperature and soot volume fraction profiles. Huang *et al.*[25] simultaneously reconstructed the multi-dimensional distributions of temperature, scattering and absorption coefficients of participating media, with the help of multi-spectral light-field imaging technique. Furthermore, Si *et al.*[27] measured the distribution of soot aggregate absorption coefficient in axisymmetric laminar ethylene diffusion flames using an imaging approach. By using

*Project supported by the National Key Research and Development Program of China (Grant No. 2017YFB0601900), the National Natural Science Foundation of China (Grant Nos. 51827808, 51821004, and 51406095), the Fundamental Research Funds for the Central Universities, China (Grant Nos. 2018ZD03 and 2017ZZD005), and Science and Technology Partnership Program, Ministry of Science and Technology of China (Grant No. KY201401003).

†Corresponding author. E-mail: liuhw@ncepu.edu.cn

© 2019 Chinese Physical Society and IOP Publishing Ltd

the particle swarm optimization (PSO) algorithm, the primary particle diameter, primary particle number, and volume fraction were presented. The two-color method adopted in the imaging method was based on Rayleigh approximation, which was fit for particles whose diameters are far smaller than the measurement wavelengths, limiting the application range of the method. By using a hyper-spectral imaging device, i.e., SOC710V, distributions of absorption coefficient under multiple wavelengths have been measured,[23] because the calculation did not rely on any approximation about particle diameter, the wavelength-dependent absorption coefficients can be used to conduct further research of particle diameter and number density.

In this paper, a diagnostics method that uses emission and scattering techniques to simultaneously determine the distributions of soot particle diameter and number density is proposed. Firstly, the experimental set-up and calculation method for the scattering measurement will be illustrated. Secondly, the algorithm and corresponding simulation verification will be introduced. Then, distributions of the particle diameter, number density, and soot volume fraction in an axisymmetric ethylene laminar diffusion flame will be experimentally determined. Finally, some conclusions will be summarized.

2. Experimental set-up

The scattering coefficients are computed by measuring the scattering and transmission laser energy. Figure 1 depicts the experiment system. An axisymmetric laminar diffusion flame is generated using ethylene and air with a co-flow laminar diffusion flame burner, consisting of a 10.9 mm inner diameter vertical tube and a 88.6 mm inner diameter concentric tube, the same as those used in Refs. [23] and [28]. A He–Ne laser device emits laser light of wavelength 632.8 nm. After being reflected by mirrors and adjusted by apertures, the laser light transfers through the flame to be studied and is eventually captured by a CCD camera (Manta G-504C). Simultaneously, the scattering energy parallel to the optical table and perpendicular to the laser transmission direction is captured by another CCD camera. Images containing and without scattering energy almost at the same time can be captured by blocking the laser light using the screen in the continuous imaging process. The flame burner is fixed on a lifting platform, providing adjustable height where the laser light transfers through the flame.

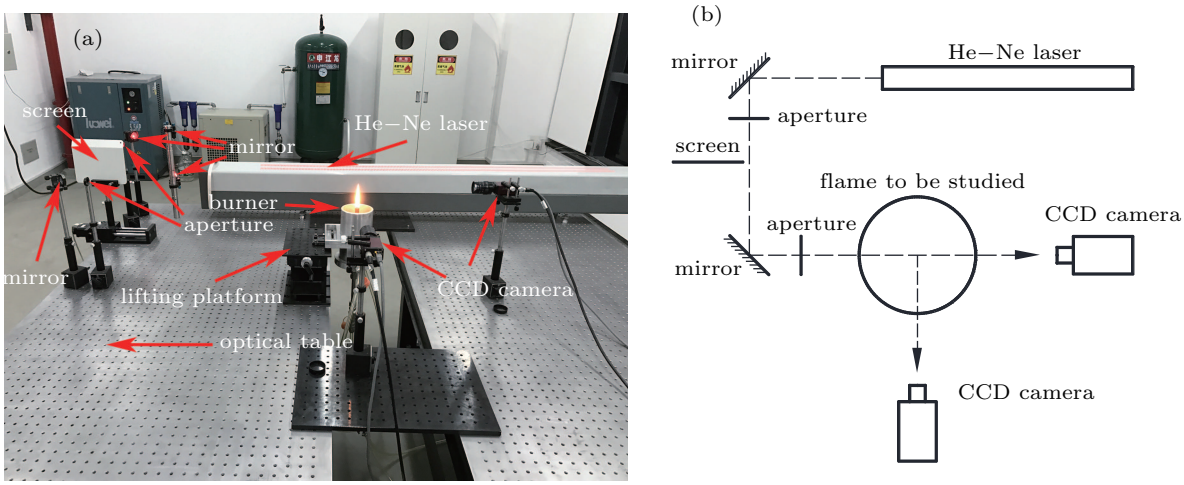


Fig. 1. Experimental set-up: (a) photograph, (b) schematic diagram.

The scattering energy for a height varies with the spatial position, corresponding to the different extinction consequences. Therefore, a CCD camera (Manta G-504C) is used to capture the transmission energy. With the transmission energy, the laser energy during transmission can be calculated using the absorption coefficients given in Ref. [23]. The steps above take the extinction effects during laser transmission into account. Similarly, the extinction effects of the scattering energy will also be considered. As shown in Fig. 2, in the corresponding spatial position, the incident laser energy I_{laser} can be calculated according to the transmission energy I_{trans} as

$$I_{\text{laser}} \cdot \exp\left(-\sum_{i=n_1}^{N_1} \kappa_i \Delta l_i\right) = I_{\text{trans}}, \tag{1}$$

where κ represents the local absorption coefficient, which can be found in Ref. [23]. Moreover, n_1 and N_1 are the starting and ending points as shown in Fig. 2, respectively, and Δl is the integral length. Similarly, in the same spatial position, the scattering energy I_{scatt} can also be computed using the energy captured by the camera $I_{\text{scatt-camera}}$ as

$$I_{\text{scatt}} \cdot \exp\left(-\sum_{j=n_2}^{N_2} \kappa_j \Delta l_j\right) = I_{\text{scatt-camera}}, \tag{2}$$

where n_2 and N_2 are the starting and ending points as illustrated in Fig. 2, respectively. The two identical cameras have the same optical property, so the ratio of the scattered energy can be evaluated, neglecting the broad response spectrum of the cameras. Accordingly, the scattering coefficients can be estimated.

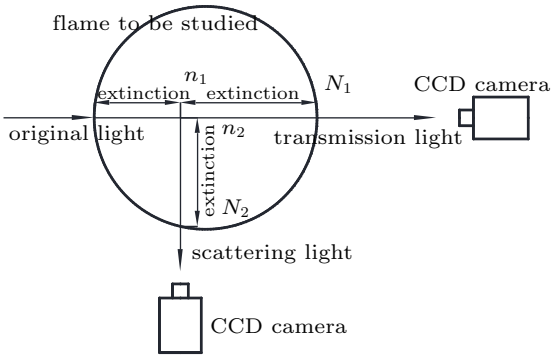


Fig. 2. Schematic diagram of the scattering process.

3. Methodology introduction and verification

3.1. Computing the particle diameter and number density

For a group of particles, given particle diameter and number density, scattering and absorption coefficients can be calculated using the Mie scattering theory.[29] Therefore, according to these two kinds of coefficients, the particle diameter and number density can be computed as well. The absorption coefficients can be measured using the imaging method. With the help of hyper-spectral imaging technique, the absorption coefficients under multiple wavelengths can be simultaneously measured. While the scattering measurement mentioned above requires an additional laser source, common laser sources can always emit laser energy under a single wavelength band. In order to reduce the complexity of the experimental system and ensure the reliability of the results, herein, the particle diameter and number density will be calculated using a search method based on the absorption coefficients under multiple wavelengths and the scattering coefficient under a single wavelength. The refractive index is referenced according to Ref. [30].

The flow chart of the search method is shown in Fig. 3. The method searches for parameter combination in the best agreement with known conditions, in a set range, with set accuracy. As shown in Fig. 3, first of all, the preliminary parameter scopes and step sizes for the particle diameter and number density should be selected, all the possible parameter combinations can be listed. Then, absorption and scattering coefficients under corresponding wavelengths for all the possible parameter combinations can be calculated using the Mie scattering theory. According to the average residual f_{resid} calculated using Eq. (3), the most consistent parameter combination with known coefficients can be elected,

$$f_{\text{resid}} = f_{\text{abs}} + f_{\text{sca}} = \sum_{i=1}^{N_\kappa} \frac{\left|\kappa_{\text{cal},i} - \kappa_i\right|}{\kappa_i \cdot N_\kappa} + \sum_{i=1}^{N_\sigma} \frac{\left|\sigma_{\text{cal},i} - \sigma_i\right|}{\sigma_i \cdot N_\sigma}, \quad (3)$$

where f_{abs} and f_{sca} are the average residuals in the absorption and scattering coefficients, respectively. N_κ and N_σ represent the numbers of these two coefficients, respectively. $\kappa_{\text{cal},i}$ and $\sigma_{\text{cal},i}$ are the absorption and scattering coefficients of the parameter combination, respectively. κ_i and σ_i demonstrate known absorption and scattering coefficients, respectively.

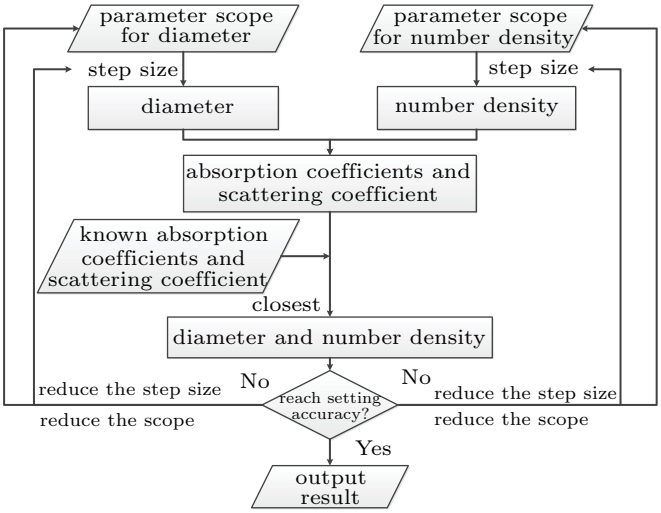


Fig. 3. Flow chart of the search method.

The elected parameter combination is the optimum solution in the set range, with the set accuracy. Around the elected parameter combination, further studies with higher accuracy can be conducted with consideration of reducing the parameter scopes and step sizes. Conducting the searching process introduced above continually results in higher and higher accuracy until reaching the desired accuracy.

3.2. Simulation verification of the search method

Given particle diameter and number density, the absorption and scattering coefficients can be computed with the help of the Mie scattering theory, which can be used to recalculate the particle diameter and number density using the search method introduced above. In the simulation, calculation is based on absorption coefficients under wavelength from 500 nm to 950 nm, with the interval of 50 nm, and scattering coefficient under wavelength 632.8 nm, in accordance with the laser device. The simulation results are shown in Table 1. In this table, the preliminary scope of the particle number density is 10^{16}–10^{18} m^{-3} and that of the particle diameter is 1–100 nm, the step sizes are 10^{16} m^{-3} and 1 nm, respectively. After achieving the most consistent parameter combination (n, d) with known conditions, the corresponding scopes and step sizes change into $(n-0.9)\times10^{16}$ m^{-3} to $(n+0.9)\times10^{16}$ m^{-3},

$(d-0.9)$ nm to $(d+0.9)$ nm, 10^{15} m^{-3}, and 0.1 nm, respectively. The desired accuracy is two digits after the decimal point. It can be seen that the mentioned method can retrieve these two parameters with good performance. The calculation times are also given in this table, which are all slightly longer than 7 s. Calculations above are undertaken with an ordinary personal computer with Intel(R) Core(TM) i7-7770 CPU and 16 GB RAM.

Table 1. Simulation verification of the search method.

No.	Set number density /10^{16} m^{-3}	Set diameter/nm	Calculated number density/10^{16} m^{-3}	Calculated diameter/nm	Calculation time/s
1	90	10	90	10	7.16
2	19	58	19	58	7.14
3	13.4	57.9	13.4	57.9	7.13
4	23.77	71.26	23.77	71.26	7.16
5	35.994	42.773	35.96	42.78	7.23
6	23.1186	56.2347	23.13	56.23	7.28

4. Data processing

Figures 4(a) and 4(b) show the flame images taken by the CCD cameras, and figures 4(c) and 4(d) display the corresponding radiation intensity images. Then the scattering signal can be computed, as shown in Fig. 5(a), and considering the attenuation effect, the scattering energy without attenuation can be calculated as well, as shown in the same figure. Figure 5(b) shows the transmission laser energy and corresponding laser energy during transmission, of which the latter is the incident laser energy for the corresponding spatial positions, i.e., the energy to be scattered. Therefore, considering the spatial range each camera pixel corresponds to, the scattering coefficients can be inferred according to the ratio of the scattering energy with approximation of isotropic scattering.

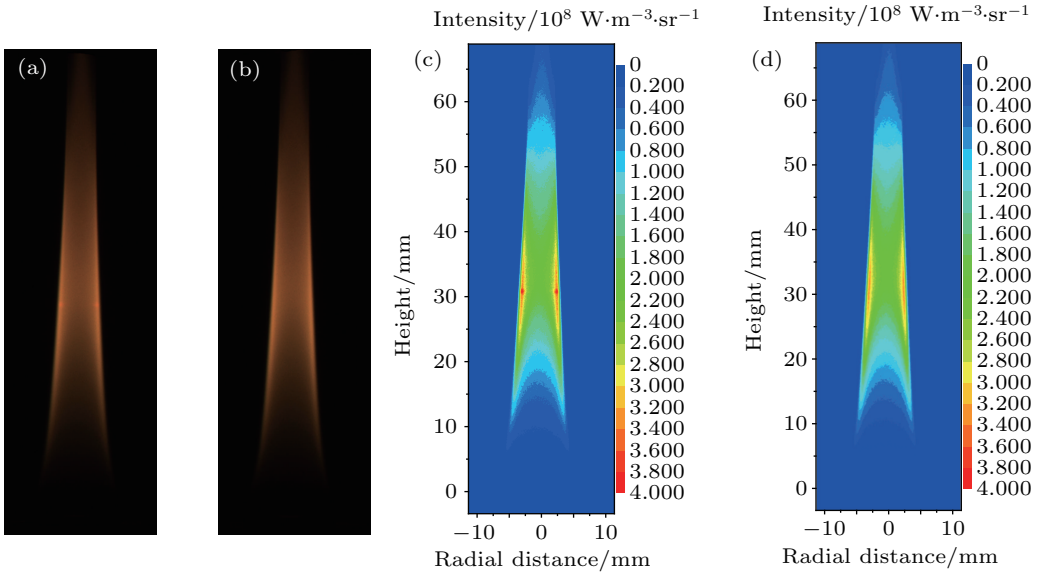


Fig. 4. Data processing for scattering signal (height = 30 mm). (a) Flame image containing scattering energy, (b) flame image without scattering energy, (c) radiation intensity containing scattering energy, (d) radiation intensity without scattering energy.

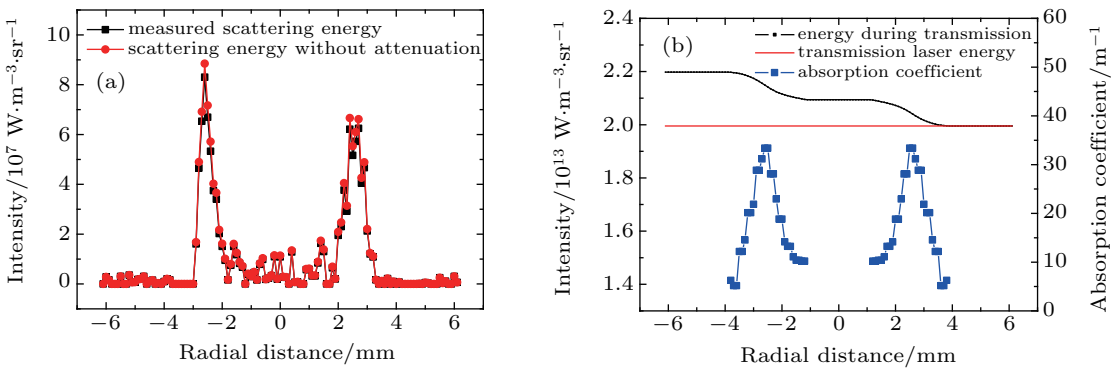


Fig. 5. Scattering energy and laser energy (632.8 nm, height = 30 mm). (a) Scattering energy, (b) corresponding incident laser energy.

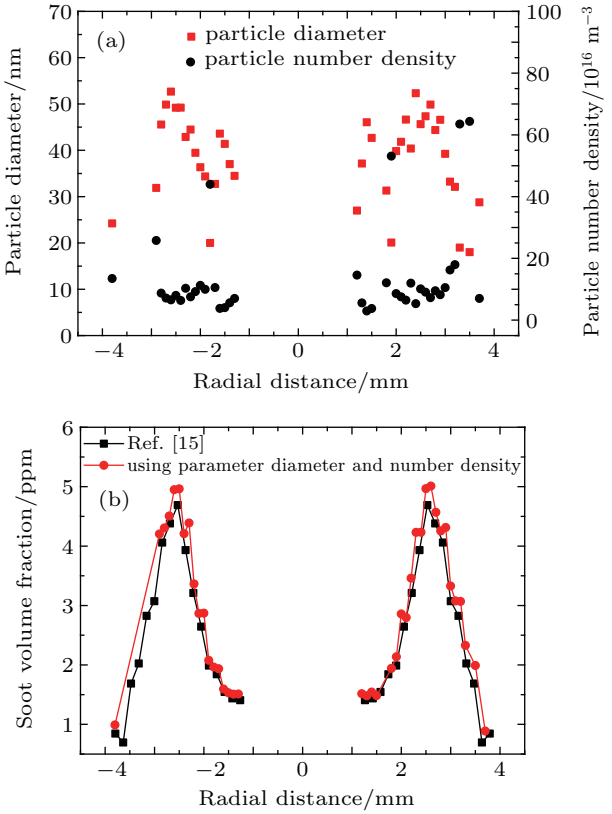


Fig. 6. Measurement results (height = 30 mm): (a) particle diameter and number density; (b) soot volume fraction.

Along with the absorption coefficients under multiple wavelengths measured in Ref. [23], the distributions of the particle diameter and number density can be estimated using the search method, as shown in Fig. 6(a). Using these two parameters, the distribution of soot volume fraction can be computed as well, as shown in Fig. 6(b). The results obtained according to the Rayleigh approximation[23] are also shown in Fig. 6(b), and the good agreement verifies the capacity of the diagnostic method.

5. Results and discussion

The flame burner is fixed on a lifting platform. Therefore, scattering coefficients at multiple heights can be measured. Figure 7 shows the scattering images at 12 different heights, i.e., from 15 mm to 70 mm, with an interval of 5 mm. The height means the distance above the burner nozzle in vertical direction. At 15 mm and 70 mm heights, the scattering energy is very weak to identify, therefore, the calculation below is directed at the other 10 heights. Figures 8(a) and 8(b) show the measurement results of the particle diameter and the particle number density, respectively. Furthermore, the soot volume fractions calculated according to the measured particle diameters and number densities are given in Fig. 8(c). Different with measurements in references, the results are calculated according to the Mie scattering theory,

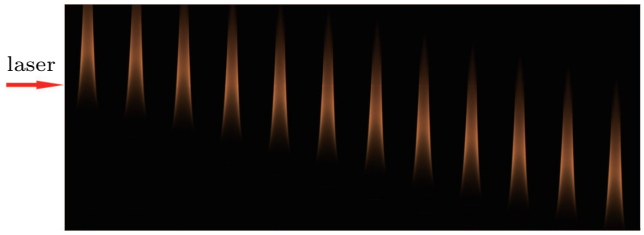


Fig. 7. Scattering images (from left to right: height = 15 mm, 20 mm, 25 mm, 30 mm, 35 mm, 40 mm, 45 mm, 50 mm, 55 mm, 60 mm, 65 mm, 70 mm).

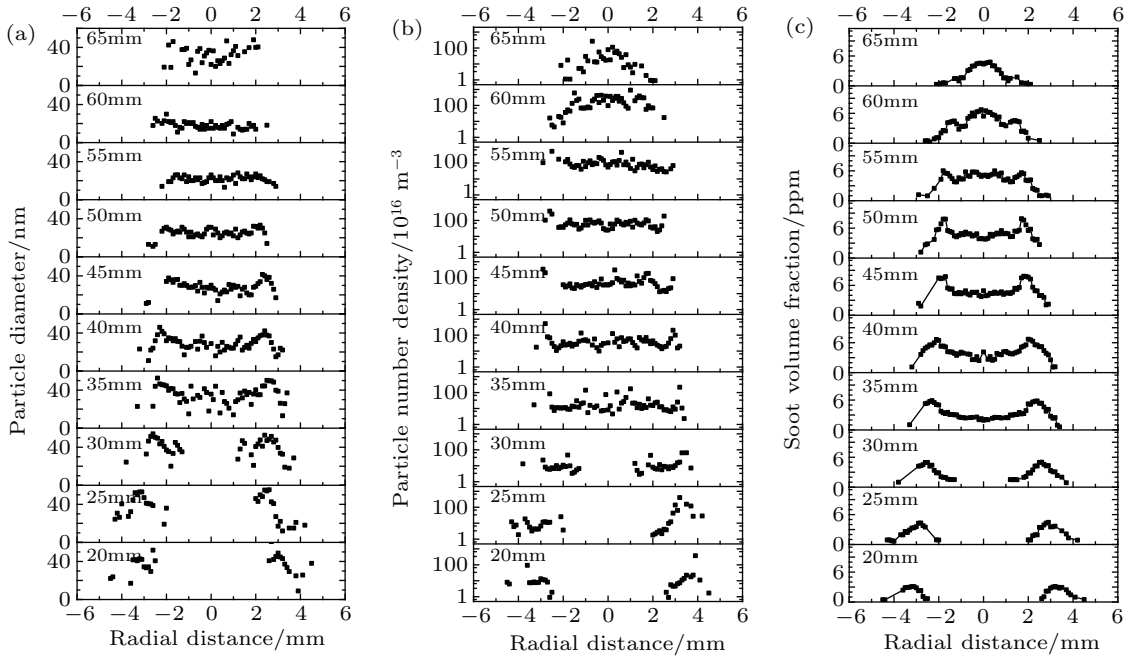


Fig. 8. Measurement results: (a) particle diameter, (b) particle number density, (c) soot volume fraction.

and are more reliable. Results show that, for ethylene laminar diffusion flame with 194 mL/min C_2H_4 and 284 L/min air, the particle diameters are in the range of 10 nm to 60 nm. In the lower part of the flame, i.e., lower than 60 mm, the distributions of particle diameter are volcano-like, similar to those of soot volume fraction, demonstrating that the higher soot volume fraction corresponds to the stronger aggregation effect. Additionally, in the higher part of the flame, as the height increases, the soot volume fraction peak in the flame center becomes increasingly clear. For the particle number density, as the height increases, in general, the particle number densities increase, up to the height 65 mm, close to the top visual area of the flame, where the number densities decrease significantly, indicating strong consumption, weak generation of soot particles due to the adequate oxidant, and strong aggregation effect due to the lower temperature near the flame edge. What is more, at the height of 65 mm, the trend in the exterior zone is more obvious than that in the flame center, demonstrating that the soot particles in the flame center will go through a similar process at higher position.

6. Conclusion

A diagnostics method using emission and scattering techniques to simultaneously determine the distribution of soot particle diameter and number density was proposed in this study. The soot particle diameters and number densities of an axisymmetric ethylene laminar diffusion flame with 194 mL/min ethylene and 284 L/min air were experimentally investigated. Firstly, scattering coefficients under 632.8 nm were experimentally measured, with consideration of the attenuation effect when laser transferred in the flame. Secondly, a search method to calculate the particle diameter and number density using absorption coefficients under multiple wavelengths and scattering coefficient under a single wavelength according to the Mie scattering theory was introduced and numerically verified. Then along with absorption coefficients under multiple wavelengths already measured, distributions of the soot particle diameter and number density at ten different heights were calculated. And using these two parameters, the distributions of soot volume fraction were given as well, which shows good agreement with those calculated according to the Rayleigh approximation. The proposed diagnostics method is proven to be capable of simultaneous determination of the distributions of soot particle diameter and number density. The conclusions are summarized as follows: (i) For ethylene laminar diffusion flame with 194 mL/min C_2H_4 and 284 L/min air, the particle diameters are in the range of 10 nm to 60 nm. (ii) In heights less than 60 mm, the distributions of particle diameter are volcano-like, similar to those of the soot volume fraction, pointing out the areas with strong aggregation effect. (iii) In heights greater than 50 mm, as the height increases, the soot volume fraction peak in the flame center becomes increasingly clear. (iv) For the particle number density, as the height increases, the particle number densities generally increase, up to the top visual area of the flame, where the number densities decrease significantly, indicating strong consumption, weak generation of soot particles due to the adequate oxidant, and strong aggregation effect due to the lower temperature near the flame edge.

References

[1] Geitlinger H, Streibel T, Suntz R and Bockhorn H 1998 *Symp. (Int.) Combustion* p. 1613
[2] Lehre T, Bockhorn H, Jungfleisch B and Suntz R 2003 *Chemosphere* **51** 1055
[3] Lehre T, Jungfleisch B, Suntz R and Bockhorn H 2003 *Appl. Opt.* **42** 2021
[4] Lee K, Han Y, Lee W, Chung J and Lee C 2005 *Meas. Sci. Technol.* **16** 519
[5] Krüger V, Wahl C, Hadef R, Geigle K P, Stricker W and Aigner M 2005 *Meas. Sci. Technol.* **16** 1477
[6] Schulz C, Kock B F, Hofmann M, Michelsen H, Will S, Bougie B, Suntz R and Smallwood G 2006 *Appl. Phys. B* **83** 333
[7] Shu X M , Fang J, Shao Q, Yuan H Y and Fan W C 2006 *Chin. Phys. Lett.* **23** 385
[8] Michelsen H, Schulz C, Smallwood G and Will S 2015 *Prog. Energy. Combust. Sci.* **51** 2
[9] He Z, Qi H, Yao Y and Ruan L 2015 *Appl. Therm. Eng.* **88** 306
[10] Gu D, Sun Z, Dally B B, Medwell P R, Alwahabi Z T and Nathan G J 2017 *Combust. Flame* **179** 33
[11] Zhao B, Yang Z, Johnston M V, Wang H, Wexler A S, Balthasar M and Kraft M 2003 *Combust. Flame* **133** 173
[12] Zhao B, Yang Z, Li Z, Johnston M V and Wang H 2005 *Proc. Combust. Inst.* **30** 1441
[13] Singh J, Balthasar M, Kraft M and Wagner W 2005 *Proc. Combust. Inst.* **30** 1457
[14] Singh J, Patterson R I, Kraft M and Wang H 2006 *Combust. Flame* **145** 117
[15] Pastor J, Garcia J, Pastor J and Buitrago J 2006 *Meas. Sci. Technol.* **17** 3279
[16] De Iuliis S, Barbini M, Benecchi S, Cignoli F and Zizak G 1998 *Combust. Flame* **115** 253
[17] Snelling D R, Thomson K A, Smallwood G J, Gülder Ö L, Weckman E J and Fraser R A 2002 *AIAA J.* **40** 1789
[18] Lou C and Zhou H C 2009 *Numer. Heat Transfer A* **56** 153
[19] Huang Q X, Wang F, Liu D, Ma Z Y, Yan J H, Chi Y and Cen K F 2009 *Combust. Flame* **156** 565
[20] Yan W and Lou C 2013 *Exp. Therm. Fluid. Sci.* **50** 229
[21] Niu C Y , Qi H, Huang X, Ruan L M , Wang W and Tan H P 2015 *Chin. Phys. B* **24** 114401
[22] Ni M, Zhang H, Wang F, Xie Z, Huang Q, Yan J and Cen K 2016 *Appl. Therm. Eng.* **96** 421
[23] Liu H, Zheng S and Zhou H 2017 *IEEE Trans. Instru. Meas.* **66** 315
[24] Yan W, Zheng S and Zhou H 2017 *Appl. Therm. Eng.* **124** 1014
[25] Huang X, Qi H, Niu C, Ruan L, Tan H, Sun J and Xu C 2017 *Appl. Therm. Eng.* **115** 1337
[26] Liu G and Liu D 2018 *Chin. Phys. B* **27** 054401
[27] Si M, Cheng Q, Song J, Liu Y, Tao M and Lou C 2017 *Combust. Flame* **183** 261
[28] Liu H, Zheng S, Zhou H and Qi C 2016 *Meas. Sci. Technol.* **27** 025201
[29] Wiscombe W J 1980 *Appl. Opt.* **19** 1505
[30] Chang H and Charalampopoulos T 1990 *Proc. Roy. Soc.* 577